PNAS RESEARCH ARTICLE | BIOPHYSICS AND COMPUTATIONAL BIOLOGY

Non-Fickian diffusion within assemblies of the intrinsically disordered protein β-casein

Laura M. Miñarro[a,b,c,1], Saikat Chakraborty[b,c,1], Christian Beck[a,c,2], Anna C. Grundel[a,d,3], Ilaria Mosca[a,c,4], Felix Roosen-Runge[e], Tatiana I. Morozova[f], Jean-Louis Barrat[b], Frank Schreiber[c], and Tilo Seydel[a,5]

Affiliations are included on p. 7.

Edited by Ken Dill, Stony Brook University, Stony Brook, NY; received November 12, 2025; accepted February 10, 2026

The molecular mechanisms governing internal fluctuations in intrinsically disordered protein (IDP) assemblies are crucial to the stability and dynamics of both regulated and aberrant toxic cellular aggregates, but remain poorly understood. By comprehensively combining high-resolution quasi-elastic neutron scattering with all-atom molecular dynamics simulations, we probe the motions of β-casein, a model IDP, inside its assemblies. We uncover a previously unresolved slow relaxation process with phenomenological characteristics of anomalous non-Fickian diffusion. This anomalous signature emerges from a continuous mobility gradient governed by density and crowding within the assemblies; the core is denser and more compact, and mobility increases progressively toward the exterior. This dynamical heterogeneity underlies the non-Gaussian behavior and accounts for the observed spectral broadening. Our findings provide insight into how disorder and extreme local crowding within IDP assemblies can result in a fundamentally different behavior compared to, e.g., clusters of well-folded proteins. The deviations from Fickian diffusion arise from dynamic heterogeneity and can be captured within the framework by a model typically used for the jump diffusion observed in liquids, thereby extending its applicability.

intrinsically disordered protein | self-assembly | short-time self-diffusion | high-resolution neutron spectroscopy | molecular dynamics simulations

Significance

Understanding how proteins move within crowded environments is essential for explaining the behavior of biomolecular condensates and other complex systems. Combining quasi-elastic neutron scattering with molecular dynamics simulations, this work uncovers the non-Fickian motion of intrinsically disordered proteins within dense assemblies, by uniquely probing the self-dynamics on pico- to nanosecond time and nanometer length scales. We propose a picture of assemblies behaving as self-crowded microenvironments, leading to anomalous diffusion and heterogeneous dynamics. This framework links molecular crowding, assembly, and transport, providing quantitative insight into how macromolecular organization can fundamentally impact diffusion processes relevant to soft matter physics and biomedical science.

Proteins are fundamental macromolecules present in living systems, responsible for a wide range of biological functions, from enzymatic activity to structural support and cellular signaling (1). Their dynamic behavior is crucial for their function, as proteins must fold, interact, and diffuse within complex, crowded cellular environments (2–6). While many proteins adopt well-defined three-dimensional structures, others, known as intrinsically disordered proteins (IDPs), do not adopt unique stable conformations under physiological conditions. This structural flexibility enables IDPs to bind to diverse partners and regulate key cellular processes, including genome organization, signal transduction, stress response, and formation of membraneless organelles (7–11). However, aberrant or irreversible aggregation of IDPs is implicated in neurodegenerative conditions such as Alzheimer's, Parkinson's, and Huntington's (12–14). Understanding the dynamics of IDP assemblies is therefore relevant both to elucidating potential functional roles and to underpinning strategies to mitigate pathological aggregation (15, 16).

Considerable progress has been made in characterizing the phase behavior and structural organization of IDP assemblies (17–20). Many IDPs form assemblies whose size, morphology, and stability are highly sensitive to environmental factors such as concentration, temperature, solvent conditions, and pH (21). These assemblies typically comprise tens to thousands of chains and display marked polydispersity. Long-time large-scale properties have been widely studied using approaches such as fluorescence microscopy, fluorescence recovery after photobleaching (FRAP) (21, 22) and dynamic light scattering (DLS), which revealed insights into aggregate size distributions (23), conformational variability, and their environmental dependence. Neutron scattering techniques, including neutron spin echo (NSE), have further clarified collective relaxation dynamics (24, 25). Together, these studies have shown that IDP assemblies remain far more dynamic than folded protein complexes (26).

Yet a crucial aspect of IDP behavior remains poorly understood, in particular, the local fluctuations on pico- to nanosecond timescales. These ultrafast motions, directly accessible by high-resolution quasi-elastic neutron scattering (QENS) (27–29), are particularly important because they govern how disordered chains fluctuate within crowded assemblies, shaping aggregate stability, maturation, surface interactions, and

[1]L.M.M. and S.C. contributed equally to this work.

[2]Present address: European Spallation Source ERIC, Data Management and Software Centre, Kongens Lyngby 2800, Denmark.

[3]Present address: Division of NanoBiotechnology, Department of Protein Science, SciLifeLab, Kungliga Tekniska Högskolan Royal Institute of Technology, Stockholm 17165, Sweden.

[4]Present address: Department of Physics and Geology, Perugia University, Perugia 06123, Italy.

[5]To whom correspondence may be addressed. Email: seydel@ill.eu.

This article contains supporting information online at https://www.pnas.org/lookup/suppl/doi:10.1073/pnas.2532636123/-/DCSupplemental.

Published March 13, 2026.

potential toxicity. Unlike folded proteins, which remain largely rigid on these timescales, IDP assemblies retain short-time flexibility (26). Despite their importance, such fast dynamics within assemblies have been extremely difficult to probe experimentally, leaving a major gap in our understanding of how molecular fluctuations give rise to the emergent properties of IDP-based assemblies.

Here, we address this challenge by combining high-resolution QENS using a latest-generation spectrometer, with all-atom molecular dynamics (MD) simulations in explicit solvent to probe the internal dynamics of IDP assemblies. Using the milk protein β-casein in aqueous solution as a representative model system (30–37), relaxation processes across multiple length and time scales are resolved by measuring and simulating the total dynamic structure factor $S(q, \omega)$. This approach separates fast local fluctuations from slower internal modes; $S(q, \omega)$ is analyzed as a function of q and $\hbar\omega$, where q denotes the absolute value of the scattering wave-vector related to the momentum transfer $\hbar q$, and $\hbar\omega$ the energy transfer. In hydrogen-rich systems, including proteins with their approximately homogeneous hydrogen distribution throughout their structure, $S(q, \omega)$ is dominated by nuclear spin-incoherent scattering, reflecting single-particle self-dynamics (27). We uncover a previously unresolved self-diffusion process where the spectral width shows a nonquadratic dependence on q, inconsistent with Fickian diffusion (38–40). This finding indicates that the motion within the assemblies deviates fundamentally from simple diffusion. Similar non-Fickian dynamics have been reported for folded proteins under conditions of extreme macromolecular crowding, created in experiments, e.g., by centrifuge removal of solvent water (41, 42), but their microscopic origin has remained elusive. Our MD simulations reproduce this behavior upon assembly, implicating dynamic heterogeneity within the assemblies as the origin of the anomalous dynamics.

Our analysis further traces the non-Fickian behavior to a radial mean-squared displacement (MSD) gradient. The suppressed displacements in the dense core and enhanced displacements at the periphery generate dynamic heterogeneity within the assembly.

Together, these results establish a general framework for understanding how assembly-induced crowding and dynamic heterogeneity shape IDP dynamics. β-casein serves here as a concrete example, but the principles likely extend broadly across disordered proteins and polyampholytes. Our findings unify anomalous diffusion (43, 44) observed in crowded biological systems with the internal fluctuations of IDP assemblies, offering insights into how disorder, crowding, and self-assembly combine to regulate protein dynamics in health and disease.

β-casein belongs to the IDP family of milk caseins comprising four major components, α_{s1}-, α_{s2}-, β-, and κ-casein, which in native milk assemble into large, hydrated colloidal micelles (45). These micelles, typically tens to hundreds of nanometers in size, are stabilized by hydrophobic interactions among casein chains and by ionic cross-linking mediated via amorphous calcium phosphate nanoclusters coordinated to phosphorylated residues. These highly dynamic, structurally heterogeneous assemblies play a central biological role in the transport and storage of calcium and phosphate. They can undergo reorganization, swelling, dissociation, or gelation depending on environmental conditions (46). β-casein is amphiphilic and, when isolated from the other casein components, retains the ability to self-associate into micelle-like assemblies in aqueous solution above a low critical micelle concentration, typically in the range of 0.5 to 2 mg mL^{-1} depending on solution conditions (36, 47, 48). These β-casein IDP assemblies are fundamentally different from native milk casein micelles: They are smaller and structurally simpler, lack the multicomponent protein composition and the inorganic calcium phosphate nanoclusters, and are therefore not stabilized by calcium–phosphate cross-linking (49). Instead, their self-assembly is driven predominantly by protein–protein interactions (50). Despite this reduced compositional complexity, β-casein assemblies remain polydisperse and sensitive to environmental conditions (37, 51). Under conditions very similar to those investigated here, previous studies have reported a characteristic mean size of the order of 8 to 15 nm for these assemblies (37, 47). In the present study, we focus exclusively on isolated β-casein assemblies, thereby enabling a direct investigation of the dynamics of a single intrinsically disordered protein species within its self-assembled structure. In the literature, the term "micelle" has been employed for these structures (52). However, since casein assemblies do not form surfactant-type micelles (37), in the following, we will use the term "assembly" for an object formed by more than one β-casein monomer chain. The high local density of these assemblies provides an element of conceptual resemblance to condensates and aggregates.

Results

Quasielastic Spectra and Non-Fickian Diffusion. We conducted a series of QENS measurements on β-casein samples at 280 K [Experiment 9-13-1046 (53)] using the IN16B spectrometer in BATS mode at the Institut Laue-Langevin (ILL). Sample concentrations ranged between 25 and 200 mg mL^{-1} in D_2O, which are well above the reported critical micelle concentration (CMC) of β-casein (0.5 to 2 mg mL^{-1}) (48). To complement the experimental data and obtain atomistic resolution of the assemblies, we performed all-atom molecular dynamics (MD) simulations with explicit solvent combining the AMBER99SB-ILDN force field and the TIP4P-D water model (54, 55). Simulated QENS spectra were generated with the *MDANSE* software (56), using protein trajectories as the input.

Fig. 1*A* provides an overview of both approaches showing the experimental sample with expected polydisperse assemblies on the *Left*, and the simulated five-chain oligomer on the *Right*. We show a typical experimental spectrum $S(q, \omega)$ in Fig. 1*B*. The wide range of $0.19\,\text{Å}^{-1} \leq q \leq 1.9\,\text{Å}^{-1}$ in IN16B resolves self-diffusion of the sample across multiple length scales (*SI Appendix*, Fig. S1). Alongside the experimental data, we present a simulated spectrum from an oligomer of five chains at a similar intermediate value of $q = 1\,\text{Å}^{-1}$. Both spectra exhibit characteristic quasi-elastic broadening, which originates from multiscale dynamic behavior at the microscopic level. The spectral broadening in simulations originates solely from protein fluctuations, whereas the experimental spectra also contain solvent water and sample container contributions. The faster solvent motion explains the broad component in Fig. 1*B* fitted by the dotted line.

Our analyses reveal that a single characteristic process is insufficient to describe the relaxation of the IDP assembly. Moreover, we find that the best-fitting model for both spectra separates the faster and slower dynamics within the assembly following

$$S(q,\omega) = \mathcal{R} \otimes \left\{ \beta \left[A_0 \mathcal{L}(\gamma, \omega) + (1 - A_0) \mathcal{L}(\gamma + \Gamma, \omega) \right] + \beta_{D_2O} \mathcal{L}(\gamma_{D_2O}, \omega) + \beta_{\text{can}} \delta(\omega) \right\} + B, \quad [1]$$

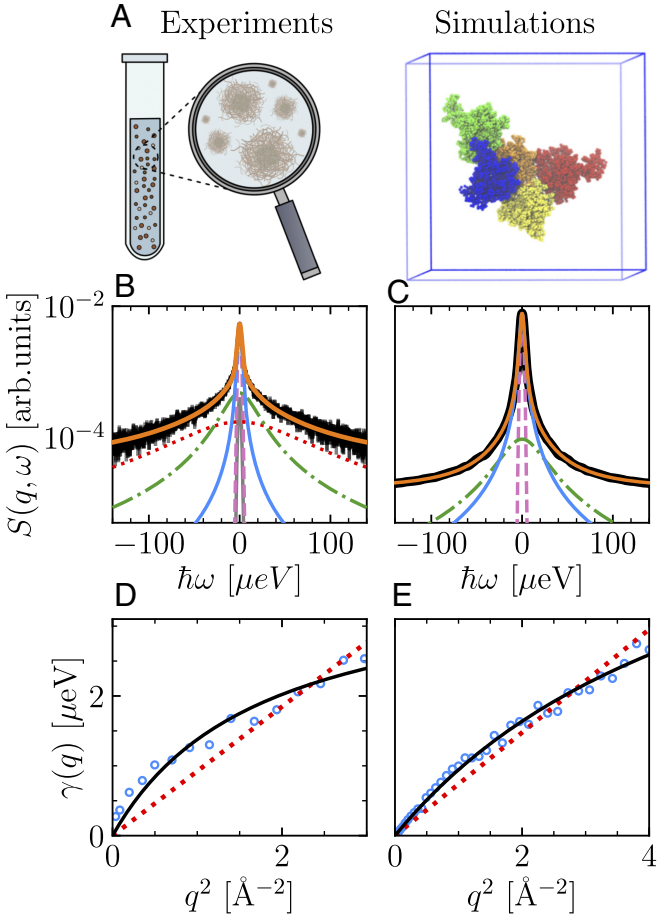

Fig. 1. (*A*) Schematic representation of experiments carried out on a sample with large assemblies in solution (*Left*) and simulations carried out on one small assembly of 5 chains (*Right*). (*B*) Experimental QENS spectrum for a 75 mg mL^{-1} β-casein sample at $q = 1.07$ Å^{-1} and (*C*) an MD-simulated spectrum for an assembly of 5 protein chains at $q = 1$ Å^{-1} and $T = 280$ K. In both spectra, the solid blue curve represents the slower contribution and the dash-dotted green curve the faster contribution; the pink dashed curve corresponds to the resolution function, and the solid orange curve to the total fit. In the experimental spectrum, solid gray and dotted red curves indicate the container and solvent contributions, respectively. (*D*) Wave-vector q^2-dependence of the half-width at half-maximum (HWHM), $\gamma(q)$, of the Lorentzian function corresponding to the slow relaxation from the experimental fit, and (*E*) from the MD simulation. The red dotted line represents the fit assuming Fickian diffusion (Eq. **2**), while the black solid line corresponds to the fit using the Singwi-Sjölander model (Eq. **3**).

where $\mathcal{L}$ denotes a Lorentzian function. The model includes the Gaussian instrumental resolution function $\mathcal{R}$, which was measured using vanadium in the experiments and fixed accordingly in the simulations. For simulations, no background and water contributions are needed, i.e., $B = 0$ and $\beta_{D_2O} = 0$. The q-dependent scalar parameters $\beta(q)$ and $A_0(q)$ account for the spectral amplitude and the elastic incoherent structure factor (EISF), respectively. For the experimental data, the additional term $\beta_{D_2O}(q)\mathcal{L}_{D_2O}(\gamma_{D_2O}(q),\omega)$ represents the contribution from the solvent, while $\beta_{can}(q)\delta(\omega)$ with the Dirac δ-function accounts for sample container contribution with the amplitude $\beta_{can}(q)$ (*SI Appendix*, Fig. S3). These terms were not subtracted but fixed based on measurements of the pure solvent and the empty container. The scalar $B(q)$ represents an apparent flat background contribution to capture ultrafast motions that lie beyond the energy range of the spectrometer.

Finally, the linewidths γ and Γ corresponding to the half-width at half-maximum (HWHM) of the two Lorentzian components, $\mathcal{L}(\gamma(q),\omega)$ and $\mathcal{L}(\gamma(q)+\Gamma(q),\omega)$, are generally associated with distinct dynamical processes in proteins occurring at different time scales (24, 57–60). The broader HWHM Γ is typically linked to rapid internal motions, whereas the narrower component γ often reflects the global diffusion of the entire protein (27). However, these interpretations are based on previous studies on folded globular proteins (FGPs), and the specific dynamics of β-casein might deviate due to its unique assembly properties and its intrinsically disordered nature.

Fig. 1 *D* and *E* depicts $\gamma(q)$ obtained from the fits using Eq. **1**, with the experimental data on the left and the simulation results on the right. In both cases, we observe a clear deviation from Fickian behavior, which corresponds to

$$\gamma(q) = Dq^2. \qquad [2]$$

The data were successfully fitted using the Singwi-Sjölander model (61),

$$\gamma(q) = \frac{Dq^2}{1+(Dq^2\tau)}, \qquad [3]$$

which was previously successfully applied, inter alia, to describe the self-diffusion of liquid water (62). Therein, D is the longer-range diffusion coefficient which is recovered as $q \to 0$ and τ is a parameter that captures the deviation from Fickian diffusion at smaller scales. In our QENS data, this deviation is observed in all samples across the concentration range measured and at all temperatures studied (*SI Appendix*, Fig. S2).

Onset of Non-Fickian Diffusion and Dynamic Heterogeneity with Assembly. To identify the origin of the anomalous diffusion, we numerically probe the differences in the dynamics for

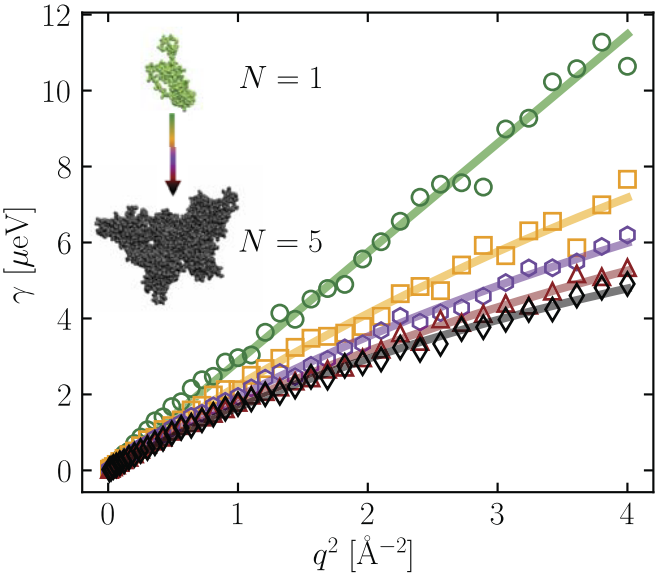

Fig. 2. q-dependence of the half-width at half-maximum (HWHM), $\gamma(q)$, of the Lorentzian corresponding to the slow contribution from the MD simulations for different protein chain assemblies (single chain in green, round symbols; $N = 2$ in orange, square symbols; $N = 3$ in violet, hexagonal symbols; $N = 4$ in brown, triangle symbols; and $N = 5$ in black, diamond symbols). Solid lines, in matching colors, represent the fits for each system, using Eq. **2** for the single chain and Eq. **3** for $N = 2$, 3, 4, and 5. The *Inset* provides a schematic representation of the transition from a single chain to an $N = 5$ assembly, illustrating the different systems analyzed.

a single chain in isolation and in assembly. We systematically increase the number of chains to $N = 5$, and study the effect on the profiles of $\gamma(q)$, see Fig. 2. An isolated protein ($N = 1$) exhibits purely Fickian $\gamma(q)$, whereas, as the number of chains increases, the deviation from Fickian diffusion becomes prominent (*SI Appendix*, Fig. S5). Moreover, D becomes smaller with increasing N, indicating a slower dynamics (*SI Appendix*, Fig. S5).

The deviation from Fickian diffusion evidenced by the nonlinear q^2-dependence of $\gamma(q)$ observed in Fig. 2 can arise due to heterogeneous mobility of the constituents of the sample (38). We explore the presence of such dynamic heterogeneities through the self-part of the van-Hove function (63, 64),

$$G_s(\mathbf{r}, t) = \frac{1}{N \cdot n_H} \left\langle \sum_{i=1}^{N \cdot n_H} \delta(\mathbf{r}_i(t) - \mathbf{r}_i(0) - \mathbf{r}) \right\rangle, \qquad [4]$$

where $\mathbf{r}_i$ denotes the position of the ith hydrogen atom at time t and $r = |\mathbf{r}|$ the distance from the origin. Here and below, $\langle \ldots \rangle$ indicates time averaging over the trajectory, and $n_H = 1{,}684$ is the number of hydrogen atoms in a single β-casein chain. Since hydrogen constitutes half of the atoms in the chain ($n_{\text{total}} = 3{,}348$), the neutron scattering signal is dominated by the incoherent scattering (~91% by cross-section), with 99.9% of this contribution arising from hydrogen.

Non-Fickian diffusion results in a non-Gaussian profile of the corresponding spherical average $G_s(r, t)$ (assuming spherical symmetry). We estimate such deviation through the non-Gaussian parameter (63, 64), $\alpha_2(t) = 3\langle r(t)^4 \rangle / 5\langle r(t)^2 \rangle^2 - 1$, and investigate the variation of α_2 with N for different values of t (*SI Appendix*, Fig. S6). Evidently, the deviation from Gaussian profile of $G_s(r, t)$ increases with growing N. The analysis reveals that self-assembly of IDPs drives dynamic heterogeneity, converting simpler single chain motion into anomalous, scale-dependent diffusion.

Crowding Effect on Protein Self-Diffusion. Fig. 3 summarizes the classical colloid picture for concentration-dependent diffusion. Within this framework, the effective diffusion coefficient at volume fraction φ is given by (65–67),

$$D(\varphi) = \frac{D_0}{1 + L(\varphi)}, \qquad [5]$$

where $D_0 = k_B T / 6\pi\eta R_h$ is the diffusion coefficient at infinite dilution, and $L(\varphi)$ the nonlinear function of φ accounting for the multibody hydrodynamic interactions. Here, R_h is the hydrodynamic radius of the diffusing unit. For β-casein, literature values from DLS and small-angle scattering give a hydrodynamic radius of $R_h^{\text{micelle}} = 8$ to 15 nm for micelles (in our work referred to as assemblies) (35, 36, 68, 69). In contrast, experimentally determining the size of monomers is more challenging due to the low CMC of this protein, which remains below 2 mg mL^{-1} under the studied conditions (48). Simulations of isolated chains yield an average monomer hydrodynamic radius of ~2.0 nm (30, 31). These correspond to dilute-limit diffusion coefficients of $D_0^{\text{micelle}} \approx 0.9$ to 1.7 Å^2/ns and $D_0^{\text{monomer}} \approx 6.8$ Å^2/ns, respectively.

In this concentration range, large changes in D are not expected: The prediction for assemblies is also relatively invariant. Still, the QENS-derived coefficients (Eqs. **1** and **3**) remain essentially concentration-independent, with a value $D \approx 2.9$ Å^2/ns that lies between the colloidal bounds for monomers and assemblies (Fig. 3). This intermediate magnitude indicates that the measured D predominantly reflects the diffusion of β-casein monomer chains within the assemblies. The alternative interpretations as global diffusion of entire assemblies or as diffusion of free monomers are inconsistent with the theoretical bounds given by single-chain and assembly diffusion (dashed and dash-dotted lines in Fig. 3, respectively).

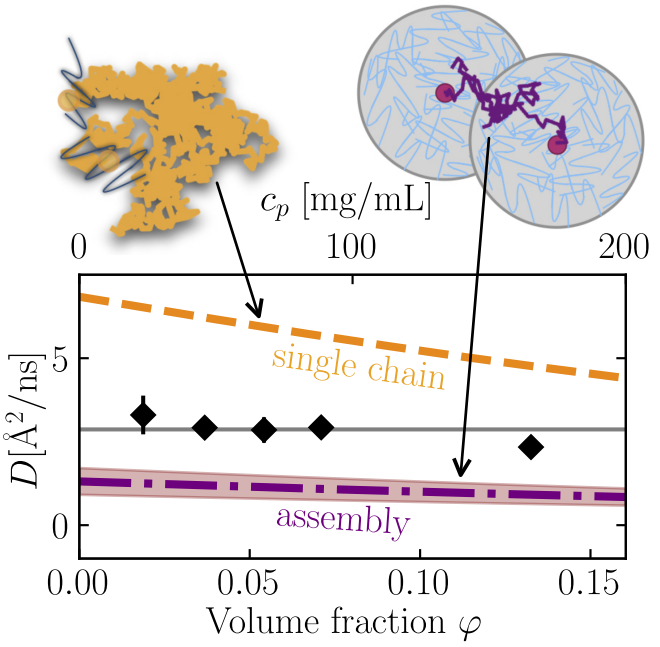

Fig. 3. Apparent diffusion coefficient D as a function of volume fraction φ (*Bottom* axis) and protein concentration c_p (*Top* axis, mg mL^{-1}) for β-casein. Black symbols denote experimental data; the solid black line marks the mean experimental D. Across the explored range, the measured D lies between the colloidal predictions for single-chain diffusion (orange dashed line) and assembly center-of-mass motion (purple dash-dotted line).

Thus, because the assemblies as a whole diffuse too slowly to be resolved by our QENS spectrometer, the measured signal predominantly reflects motions within the assemblies. We therefore interpret the observed diffusion coefficient as arising from the effective motion of individual β-casein chains within the assemblies, which is hindered relative to free monomers in solution but remains significantly faster than the center-of-mass diffusion of the assemblies themselves.

An alternative model, which accounts for a single effective global contribution resulting from a superposition of assembly and free monomer diffusion, led to unphysical fit parameters (cf. *SI Appendix*). Our interpretation attributing the narrow Lorentzian $\gamma(q)$ in our fits of Eq. **1** to monomer diffusion within the assemblies is further supported by all-atom molecular dynamics simulations of a small β-casein assembly ($N = 5$ chains), which yield diffusion coefficients in close agreement with the experimental values (*SI Appendix*, Fig. S5). Although finite-size effects and periodic boundary conditions may slightly underestimate D, the consistency between simulations and experiments—despite the vastly different assembly sizes—confirms that QENS primarily probes the non-Fickian chain diffusion within dense assemblies.

Origin of Dynamic Heterogeneity and Self-Induced Supercrowding. For atomistic insight into the dynamic heterogeneity, we track the MSD $\delta r_i^2(t) = \langle [\mathbf{r}_i'(t) - \mathbf{r}_i'(0)]^2 \rangle$ with $i = 1..$

$(N \cdot n_H)$ of the hydrogen atoms in the assembly. To remove the translation of the center-of-mass (COM) of the assembly, we use coordinates in the COM frame: $\mathbf{r}'_i = \mathbf{r}_i - 1/(N \cdot n_H) \sum_i \mathbf{r}_i$ for the computation of δr_i^2. We highlight the mobility of these atoms, coloring them according to their δr_i^2 values, see Fig. 4*A*, for $t = 1$ ns. The segments closer to the core of the assembly seem to have low mobility, whereas the hydrogen atoms closer to the surface display faster motion.

To quantify such radially differential mobility, we partition the 5-chain assembly into concentric shells of equal width $\Delta R = 1$ nm and inner radii $R_{\mathrm{COM}} = K \cdot \Delta R$ $(K = 0...5)$ around the COM of the assembly, see Fig. 4*B*. A shell K contains $k = 1...N_K$ hydrogen atoms at distances $R_K = \{R_k | K \cdot \Delta R \leq R_k < (K+1) \cdot \Delta R\}$. The MSD of the hydrogen atoms residing within a shell $\Delta r_K^2(R_{\mathrm{COM}}, t) = 1/N_K \sum_{k=1}^{N_K} \delta r_k^2(t)$ probes the mobility corresponding to the shell at a distance R_{COM} from the COM of the assembly. Due to internal fluctuations, atoms belonging to a shell, particularly close to the edge, may infiltrate its neighboring shells. However, at short times $t \approx 1$ ns corresponding to the time resolution of QENS, for the configurational average $\delta r^2(t) := 1/(N \cdot n_H) \sum_{i=1}^{N \cdot n_H} \delta r_i^2$ we find

$$\delta r^2(t) \approx \frac{\sum_{R_{\mathrm{COM}}=0}^{R_{\mathrm{COM}}^{\max}} N_K \Delta r^2(R_{\mathrm{COM}}, t)}{\sum_{R_{\mathrm{COM}}=0}^{R_{\mathrm{COM}}^{\max}} N_K} \quad [6]$$

(*SI Appendix*, Fig. S7). The proximity of the two MSD profiles establishes that atomic movements across shells do not significantly disrupt the shell partitioning at times under consideration. With increasing distance from the assembly COM, a monotonic rise of $\Delta r^2(R_{\mathrm{COM}}, t)$ can be observed for different values of t (*SI Appendix*, Fig. S7). We color the shells in Fig. 4*B* for $t = 1$ ns

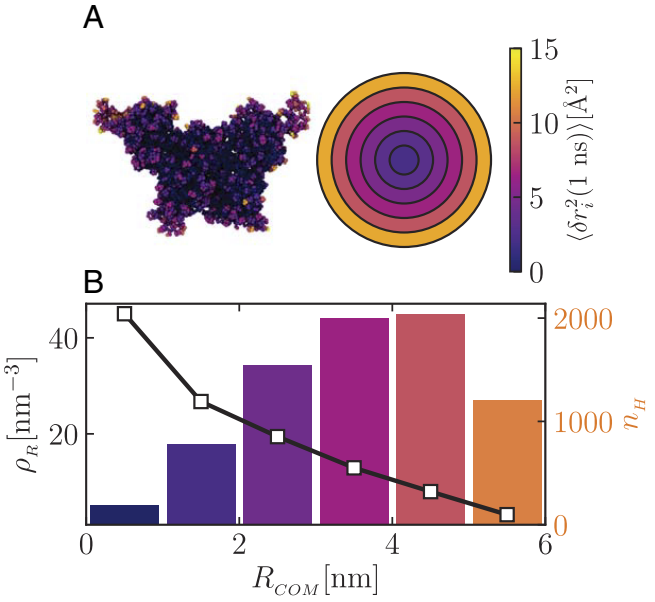

Fig. 4. (*A*) *Top Left*: Mobility $\langle \delta r_i^2 \rangle$ of the atoms within an assembly of 5 chains color-coded per the color bar on the far *Right*. *Top Right*: Shell model describing this heterogeneous dynamics in the assembly, using the same color code. (*B*) Number density ρ_R of hydrogen atoms (black line, *Left* y-axis) and number of hydrogen atoms n_H (histogram, *Right* y-axis) per shell versus the distance R_{COM} from the center-of-mass of the assembly, illustrating the supercrowding close to the core as evidenced by the profile of ρ_R. The colors in the histogram reflect the shell model shown above for easier visual correspondence and relate to the respective mobility.

to visually distinguish the mobility of different shells. Clearly, the radial variation in mobility of the protein residues is the origin of the observed dynamic heterogeneity in the assemblies.

To understand the heterogeneous situation within the assembly, in Fig. 4*B*, we show the histogram of N_K and variation of number density $\rho_R = N_K / 4\pi R_{\mathrm{COM}}^2 \Delta R$ with R_{COM}. The value of ρ_R close to the core is significantly larger than the bulk number density in simulations $n_H / L_{\mathrm{box}}^3 \approx 1.3\ \mathrm{nm}^{-3}$. Assuming even distribution of hydrogen atoms in the assembly, the value of ρ_R for $R_{COM} = 1$ nm corresponds to a mass concentration of ~1,093 mg/mL. This value can be compared to the highest protein concentrations of ~600 mg/mL for crowding studies of FGPs (58). Thus, we see signatures of supercrowding close to the core. The radially outward monotonic decay of $\rho_R(R_{COM})$ indicates structural heterogeneity within the assembly.

Disentangling Components of the Non-Fickian Diffusion. We have established that assembly leads to strong deviations from simple Fickian behavior in $\gamma(q)$, driven by self-crowding that produces radial variations in mobility within the assemblies. A key question is whether such spatial heterogeneity alone can explain the observed anomalies, or whether additional factors are required (38, 40, 70). Previous studies on FGPs suggest that dynamic heterogeneity by itself can give rise to anomalous diffusion, even within a Gaussian framework (38, 40). At the same time, research on crowded systems has shown that non-Gaussian corrections are also crucial, as they capture deviations from simple diffusion statistics and are hallmarks of anomalous transport (43).

To assess the relative contributions of these factors, we analyze the incoherent intermediate scattering function $I(q, t)$, which is well suited for spectral information in real time,

$$I(q,t) = \int_{-\infty}^{+\infty} S(q,w) e^{-j\omega t} d\omega = \frac{1}{N \cdot n_H} \sum_{i=1}^{N.n_H} \left\langle \exp\left[j\mathbf{q} \cdot (\mathbf{r}'_i(t) - \mathbf{r}'_i(0)) \right] \right\rangle. \quad [7]$$

As we extend the shell-based model for the following analyses, we continue to work with the coordinates $\mathbf{r}'_i$ in the COM frame of the assembly. Assuming statistical equivalence of MSD of the hydrogen atoms and isotropic environment within a shell, the Gaussian approximation reduces Eq. 7 to

$$I_{HM}(q,t) = \frac{1}{N \cdot n_H} \sum_K \exp\left[-\frac{q^2}{6} \Delta r_K^2(R_{\mathrm{COM}}, t) \right]. \quad [8]$$

This formulation preserves spatial resolution at shell-level, thereby enabling direct assessment of the impact of heterogeneous mobility (HM) on $\gamma(q)$.

Incorporating deviations from Gaussian displacement statistics, the intermediate scattering function can be expanded to include the leading-order non-Gaussian (NG) correction, yielding

$$I_{NG}(q,t) = \frac{1}{N \cdot n_H} \sum_K \exp\left[-\frac{q^2}{6} \Delta r_K^2(R_{\mathrm{COM}}, t) + \frac{q^4}{72} \alpha_2(t) \left\langle \Delta r_K^2(R_{\mathrm{COM}}, t) \right\rangle^2 \right]. \quad [9]$$

Physically, this correction represents locally non-Fickian effects within the shell, including transient caging and subdiffusive motion, which are neglected in the Gaussian approximation. To avoid the spurious long-time growth of $I(q,t)$ introduced by truncating the cumulant expansion at this order, we restrict the validity of Eq. **9** to small q, where the expansion remains well-behaved. Within this regime, the inclusion of the non-Gaussian term provides a more accurate characterization of dynamical heterogeneity while preserving a tractable analytical form.

For completeness, removal of spatial resolution and non-Gaussian correction reduces Eq. **7** to the uniform mobility (UM) limit,

$$I_{UM}(q,t) = \exp(-q^2\delta r^2(t)/6), \qquad [10]$$

where $\delta r^2(t) = \sum_{i=i}^{N.n_H} \delta r_i^2$ is the assembly-averaged MSD of the hydrogen atoms. This expression assumes spatially homogeneous, globally Fickian dynamics and therefore provides the natural baseline against which the effects of shell-resolved dynamics (Eqs. **8** and **9**) can be compared.

Finally, the q dependent spectral broadening $\gamma(q)$ in frequency space is inversely proportional to the characteristic relaxation time $\tau(q)$ that describes the decay of $I(q,t)$: $I(q,t) = \exp(-t/\tau(q)) = \exp(-\gamma(q)t)$. We compute $I_x(q,t)$, $x = HM,\ NG,\ UM$ using Eqs. **8**–**10**. Next, we estimate $\gamma(q)$ following

$$\gamma_x(q) = \left\langle \frac{d}{dt} \ln I_x(q,t) \right\rangle, \qquad [11]$$

with $x = HM,\ NG,\ UM$.

Fig. 5 compares $\gamma(q)$ obtained from the three approaches above (symbols) with values computed directly from molecular dynamics trajectories without any analytical approximation (solid line). The profile of $\gamma_{UM}(q)$ exhibits purely Fickian behavior. The results directly calculated from the molecular dynamics trajectories (solid line in Fig. 5) closely follow the shell-resolved Gaussian prediction γ_{HM}, although they exhibit slightly greater deviations from ideal Fickian scaling. By contrast, inclusion of only the first-order non-Gaussian correction in γ_{NG} yields substantially stronger deviations, suggesting that higher-order corrections are necessary for quantitative agreement with simulations. These findings demonstrate that spatial heterogeneity in mobility and non-Gaussian effects both contribute to the observed spectral broadening. Importantly, $\gamma(q)$ remains non-Fickian even when the individual shells are modeled as purely Fickian diffusers with diffusion coefficients consistent with their MSDs (*SI Appendix*, Fig. S8), showing that an ensemble of locally Fickian components can nonetheless produce globally non-Fickian dynamics.

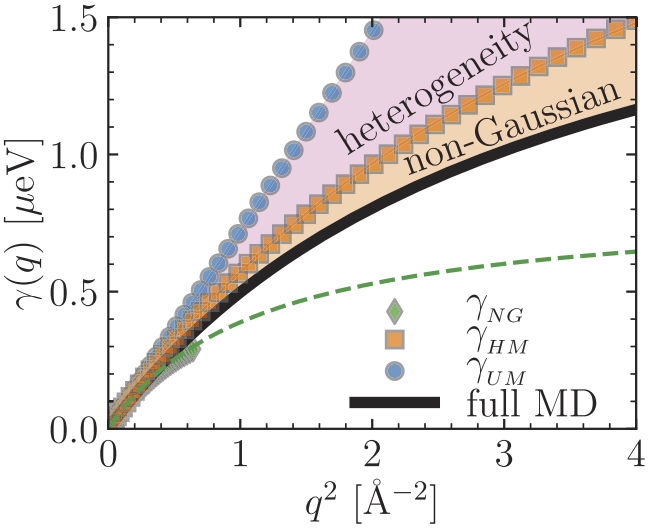

Fig. 5. Contributions of heterogeneous mobility (HM), non-Gaussian corrections (NG), and the uniform Gaussian mobility (UM) to the observed deviation from Fickian diffusion evidenced by the nonlinear q^2-dependence of the linewidth $\gamma(q)$. Results are benchmarked against direct calculations from fully atomistic MD trajectories using MDANSE (solid line labeled "full MD"). Here, $\gamma_x(q)$, $x = HM,\ NG,\ UM$, are obtained from the corresponding intermediate scattering functions $I_x(q,t)$ using Eqs. **8**, **9**, and **11**, where HM accounts for shell-resolved mobility, NG incorporates leading-order non-Gaussian displacement statistics, and UM assumes spatially homogeneous, globally Fickian dynamics. While heterogeneous mobility is sufficient condition for inducing non-Fickian diffusion, our system has non-Gaussian corrections as well.

Discussion

IDPs are increasingly being recognized as the central components in cellular organizations, where their assemblies drive both functional compartmentalization and pathological aggregation. A major unresolved question has been how pico- to nanoseconds internal relaxations of these assemblies shape their emergent dynamics. By combining high-resolution QENS and atomistic MD simulations, we demonstrate that IDP assemblies naturally generate self-diffusion coefficients given by Eq. **3** rather than by Eq. **2**, a defining signature of non-Fickian diffusion. Such features were previously observed in systems of well-folded proteins and colloids with high bulk or external crowding but lacked mechanistic insights.

Our results show that assembly itself is sufficient to induce such anomalous diffusion by compartmentalizing a crowded environment, even in the absence of bulk crowding. Our simulations reveal that the observed non-Fickian behavior arises from a direct coupling between structural and dynamic heterogeneity within the assemblies. The dense, solvent-excluded core creates a supercrowded environment where fluctuations are strongly suppressed, while residues near the periphery remain more mobile. This radial gradient in density and mobility produces heterogeneous dynamics that cannot be captured by a simple Gaussian description. To account for these deviations, non-Gaussian corrections become essential. These corrections quantify departures from random-walk statistics, highlight the role of intermittent or rare events, and expose higher-order correlations that shape transport in crowded systems. Together, the interplay of structural confinement and dynamic heterogeneity, amplified by non-Gaussian effects, explains the anomalous spectral broadening and establishes assembly-induced crowding as a robust route to non-Fickian diffusion.

These findings establish a unifying framework for interpreting anomalous diffusion in protein systems. They suggest that signatures of non-Fickian dynamics experimentally observed earlier in artificially solvent water-depleted solutions of folded proteins (41, 42, 71), may arise from the same physical principle of crowding-induced spatial heterogeneity in mobility. IDP assemblies provide a natural testbed for this phenomenon because they reproduce the essential features of supercrowded environments while retaining short-time flexibility. The mentioned previous reports of non-Fickian $\gamma(q)$ profiles have typically been associated with systems at extremely high concentrations, created, e.g., by solvent water depletion through centrifuging, suggesting that these extreme crowding effects may underlie such behavior (41, 42, 71). Simultaneously, for several FGPs, this concentration dependence has been successfully described within a colloid framework when the proteins were fully dissolved: Increasing protein concentration (self-crowding) or adding external

crowding agents both reduce the effective diffusion coefficient, while remaining consistent with Fickian diffusion over a broad range around physiological total volume fractions (3, 58). This consistency with the colloid picture also holds when the FGPs form clusters, both experimentally (59, 72, 73) and in simulations (74). In these studies investigating inter alia lysozyme, bovine serum albumin, β-lactoglobulin, as well as monoclonal antibody solutions, the FGP clusters were found rigid on the nanosecond time scale, while being possibly transient on much longer time scales (59, 72, 74, 75). In contrast, our system of β-casein assemblies constitutes a model where dynamical heterogeneity naturally governs protein chain diffusion within these assemblies already on the nanosecond time scale, which we attribute to the flexibility of the IDP chains compared to the relative rigidity of clusters formed by FGPs. Deviations from Fickian diffusion due to cage effects for crowded FGP solutions have only been observed on much longer time scales (76).

More broadly, our work highlights how the interplay of disorder, crowding, and self-assembly creates complex dynamical behavior that deviates from classical diffusion theory. Thus, the framework we propose bridges protein biophysics with concepts from polymer and soft-matter physics such as dynamic heterogeneity (77), self-assembly (78), and multiscale diffusion (16), offering a general picture of how anomalous signatures emerge in extremely crowded biomolecular systems. The non-Fickian diffusion in extremely dense IDP assemblies, thus, adds an important complement to the colloid picture holding in a wide range around average physiological concentration of FGPs. The simultaneous access to spatial and time correlations on the nanosecond time and nanometer length scale permits to quantify a non-Fickian diffusion mechanism relevant for the contemporary discussion of anomalous transport in biological cells (44). In addition to quantitatively describing a diffusion mechanism, our work also confirms the highly dynamical character of a very dense IDP assembly. This rapid dynamics has been identified as a requirement for biomolecular rearrangements underlying efficient reactions at the molecular scale (15). The importance of this nanoscale dynamics for permitting biological function has been further pointed out, e.g., for biomolecular condensates consisting of IDPs (16). The non-Fickian diffusion within dense assemblies of disordered proteins may be assumed to impact on biochemical reaction rates, signal transduction, and intracellular organization.

Materials and Methods

β-casein from bovine milk (Prod. No. C6905, BioUltra ≥98% purity) was purchased as lyophilized powder from Sigma-Aldrich of Merck KGaA (Darmstadt, Germany). The product contains at least 75% protein by the Biuret method, with over 98% of that protein being pure β-casein, resulting in a minimum of 73.5% β-casein in the total product. Mass spectrometry measurements confirmed the purity of the proteins. The samples were prepared by dissolving the protein in 25 mM sodium phosphate buffer prepared in D_2O without agitation at 5 °C. The total dissolution time is 24 h on average. The pD was adjusted to 7.3 ± 0.1 using small amounts of 1 M DCl or 1 M NaOD, at final protein concentrations ranging from 25 to 200 mg mL^{-1}. Just before the measurements, the samples were loaded into aluminum cylindrical sample holders (15 mm outer diameter, 0.3 mm gap) and brought to the measurement temperature of 280 K.

Neutron Backscattering. We used the cold neutron backscattering spectrometer IN16B (28, 79, 80) at the Institut Laue-Langevin in Grenoble, France, in the inverted time-of-flight (BATS) configuration with Si(111)-analyzer crystals (Exp. 9-13-1046) with a chopper setting achieving ∼3.5 μeV FWHM Gaussian energy resolution at an elastic wavelength of 6.27 Å.

Atomistic Molecular Dynamic Simulations. We performed all-atoms MD simulations at $T = 280$ K in explicit water using *GROMACS* 2023 package (81). The interactions in simulations were set using AMBER99SB-ILDN force-field in combination with the TIP4P-D water model. The simulation with $N = 5$ chains starts from an assembled conformation in a simulation box of size $L_{box} \approx 18.62$ nm, obtained from a preliminary simulation which started with the chains being randomly placed in the box. This is followed by a 500 ns run in an NPT ensemble (*SI Appendix*, Fig. S4). We present results for the work from two subsequent 500 ns long simulation starting from randomly chosen initial configurations from the simulations in NPT ensemble. We use the NVT ensemble to avoid box artifacts of length fluctuations on dynamic observables.

Initial configurations for simulations with $N < 5$ are generated by removing appropriate number of proteins from 5 chain assemblies. We initiate the simulations in cubic boxes with at least 2.5 nm distance between the configuration and the walls, solvate the box with water and add counterions (8 Na^+ ions for each protein molecule) to attain charge neutrality. The resulting system passes through energy minimization, and short NVT and NPT runs to find a local minimum to stabilize the simulation. We use NPT equilibration runs for at least 150, 200, 300, and 400 ns for $N = 1, 2, 3$, and 4, respectively. Once again, the dynamic data are extracted from following NVT simulations.

All bonds were constrained using the LINCS algorithm. The Verlet leapfrog algorithm was used to numerically integrate the equations of motion with a time step of 2 fs. A cutoff of 1.2 nm was used for short-range electrostatic and Lennard-Jones interactions. Long-range electrostatic interactions were calculated by particle–mesh Ewald summation with a fourth-order interpolation and a grid spacing of 0.16 nm. The solute and the solvent were coupled separately to a temperature bath of 280 K using a velocity-rescaling thermostat with a relaxation time of 0.1 ps. For NPT simulations, the pressure was fixed at 1 bar using the Parrinello–Rahman algorithm with a relaxation time of 2 ps and isothermal compressibility of 4.5×10^{-5} bar^{-1}. In NVT simulations, we turned off the pressure coupling.

We transformed and analyzed the trajectory using inbuilt modules of *gmx* in *GROMACS*. BATS like spectra were generated using *MDANSE* software (56). For drawing simulation snapshots, we utilized VMD. Alongside, home-grown Python code has been used to read the files, interpret results, and generate plots.

Data, Materials, and Software Availability. All neutron data are permanently curated by the ILL and accessible under DOI: 10.5291/ill-data.9-13-1046 (53).

ACKNOWLEDGMENTS. We are grateful for stimulating discussions with Olga Matsarskaia (ILL) and Harish Srinivasan (University of Tübingen). Moreover, the authors acknowledge funding by the Deutsche Forschungsgemeinschaft (DFG)-Agence Nationale de la Recherche (ANR) German-French collaborative grant IDPXN (ANR-21-CE06-0047/DFG SCHR700/42-1) and by the Bundesministerium für Bildung und Forschung (BMBF) (ErUM-pro 05K19VTB and 05K22VTA). We performed numerical simulations on GPU-accelerated partitions of the Jean Zay supercomputer hosted by Grand équipement national de calcul intensif (GENCI)-Institute for Development and Resources in Intensive Scientific Computing (IDIRIS) (project AD010914227). L.M.M. and S.C. acknowledge PhD and Postdoctoral fellowships, respectively, funded by the ANR and DFG within the IDPXN project. C.B. acknowledges a postdoctoral fellowship funded by the BMBF, I.M. an ILL PhD studentship funded by InnovaXN, a European Union (EU) Horizon 2020 Marie Skłodowska-Curie Actions (MSCA) COFUND Programme (Grant No. 847439), and A.C.G. an ILL student placement.

Author affiliations: [a]Institut Max von Laue – Paul Langevin, Science Division, Grenoble 38042, France; [b]Laboratoire Interdisciplinaire de Physique, Université Grenoble-Alpes, CNRS, Saint-Martin-d'Hères 38402, France; [c]Institut für Angewandte Physik, Universität Tübingen, Tübingen 72076, Germany; [d]Fakultät für Physik und Astronomie, Universität Heidelberg,Heidelberg 69117, Germany; [e]Division of Physical Chemistry, Lund University, Lund 22100, Sweden; and [f]CNRS, Ecole Normale Supérieure de Lyon, Laboratoire de Physique, UMR5672, Lyon 69342, France

Author contributions: F.R.-R., T.I.M., J.-L.B., F.S., and T.S. designed research; L.M.M., S.C., C.B., A.C.G., I.M., and T.S. performed research; L.M.M., S.C., and A.C.G. analyzed data; and L.M.M., S.C., C.B., F.R.-R., T.I.M., J.-L.B., F.S., and T.S. wrote the paper.

The authors declare no competing interest.

This article is a PNAS Direct Submission.

1. P. E. Wright, H. J. Dyson, Intrinsically disordered proteins in cellular signalling and regulation. *Nat. Rev. Mo. Cell Biol.* **16**, 18–29 (2015).
2. D. Thirumalai, D. K. Klimov, G. H. Lorimer, Caging helps proteins fold. *Proc. Natl. Acad. Sci. U.S.A.* **100**, 11195–11197 (2003).
3. M. Grimaldo *et al*., Protein short-time diffusion in a naturally crowded environment. *J. Phys. Chem. Lett.* **10**, 1709–1715 (2019).
4. H. Frauenfelder, S. G. Sligar, P. G. Wolynes, The energy landscapes and motions of proteins. *Science* **254**, 1598–1603 (1991).
5. O. Keskin, A. Gursoy, B. Ma, R. Nussinov, Principles of protein-protein interactions: What are the preferred ways for proteins to interact? *Chem. Rev.* **108**, 1225–1244 (2008).
6. E. Fagerberg, P. Holmqvist, S. Lenton, P. Pernot, M. Skepö, Minimal structural perturbation of histatin 5 in crowded environments: Insights from small-angle x-ray scattering, dynamic light scattering, and computer simulations. *J. Colloid Interface Sci.* **700**, 138310 (2025).
7. N. Sekiyama, R. Kobayashi, T. S. Kodama, Toward a high-resolution mechanism of intrinsically disordered protein self-assembly. *J. Biochem.* **174**, 391–398 (2023).
8. K. K. Turoverov *et al*., Stochasticity of biological soft matter: Emerging concepts in intrinsically disordered proteins and biological phase separation. *Trends Biochem. Sci.* **44**, 716–728 (2019).
9. V. N. Uversky, Intrinsically disordered proteins in overcrowded milieu: Membrane-less organelles, phase separation, and intrinsic disorder. *Curr. Opin. Struct. Biol.* **44**, 18–30 (2017).
10. A. L. Darling, Y. Liu, C. J. Oldfield, V. N. Uversky, Intrinsically disordered proteome of human membrane-less organelles. *Proteomics* **18**, 1700193 (2018).
11. Y. Jo, Y. Jung, Interplay between intrinsically disordered proteins inside membraneless protein liquid droplets. *Chem. Sci.* **11**, 1269–1275 (2020).
12. E. Montejo, L. de Garcini, J. Avila Serrano, Self assembly of microtubule associated protein tau into filaments resembling those found in Alzheimer disease. *Biochem. Biophys. Res. Commun.* **141**, 790–796 (1986).
13. M. R. Cookson, α-synuclein and neuronal cell death. *Mol. Neurodegener.* **4**, 9 (2009).
14. M. Goedert, Alzheimer's and Parkinson's diseases: The prion concept in relation to assembled Aβ, tau, and α-synuclein. *Science* **349**, 1255555–1–1255555–9 (2015).
15. N. Galvanetto *et al*., Extreme dynamics in a biomolecular condensate. *Nature* **619**, 876–883 (2023).
16. N. Galvanetto *et al*., Material properties of biomolecular condensates emerge from nanoscale dynamics. *Proc. Natl. Acad. Sci. U.S.A.* **122**, e2424135122 (2025).
17. J. R. Simon, N. J. Carroll, M. Rubinstein, A. Chilkoti, G. P. López, Programming molecular self-assembly of intrinsically disordered proteins containing sequences of low complexity. *Nat. Chem.* **9**, 509–515 (2017).
18. H. Y. J. Fung, M. Birol, E. Rhoades, IDPs in macromolecular complexes: The roles of multivalent interactions in diverse assemblies. *Curr. Opin. Struct. Biol.* **49**, 36–43 (2018).
19. U. Baul, D. Chakraborty, M. L. Mugnai, J. E. Straub, D. Thirumalai, Sequence effects on size, shape, and structural heterogeneity in intrinsically disordered proteins. *J. Phys. Chem. B* **123**, 3462–3474 (2019).
20. F. Garcia Quiroz *et al*., Intrinsically disordered proteins access a range of hysteretic phase separation behaviors. *Sci. Adv.* **5**, eaax5177 (2019).
21. F. X. Theillet *et al*., Physicochemical properties of cells and their effects on intrinsically disordered proteins (IDPs). *Chem. Rev.* **114**, 6661–6714 (2014).
22. J. V. Silva, S. Pezennec, S. Lortal, J. Floury, Flexibility and charge of solutes as factors that determine their diffusion in casein suspensions and gels. *J. Agric. Food Chem.* **63**, 6624–6632 (2015).
23. M. K. Białobrzewski *et al*., Diversity of hydrodynamic radii of intrinsically disordered proteins. *Eur. Biophys. J.* **52**, 607–618 (2023).
24. A. M. Stadler *et al*., Internal nanosecond dynamics in the intrinsically disordered myelin basic protein. *J. Am. Chem. Soc.* **136**, 6987–6994 (2014).
25. F. Ameseder *et al*., Structure and dynamics of intrinsically disordered and unfolded proteins: Investigations using small-angle scattering and neutron spin-echo spectroscopy. *Biophys. J.* **116**, 490a–491a (2019).
26. Z. Liu, Y. Huang, Advantages of proteins being disordered. *Protein Sci.* **23**, 539–550 (2014).
27. M. Grimaldo, F. Roosen-Runge, F. Zhang, F. Schreiber, T. Seydel, Dynamics of proteins in solution. *Q. Rev. Biophys.* **52**, e7 (2019).
28. C. Beck *et al*., Neutron spectroscopy on protein solutions employing backscattering with an increased energy range. *Phys. B Condens. Matter* **562**, 31–35 (2019).
29. V. K. Sharma, S. Mitra, R. Mukhopadhyay, Dynamic landscape in self-assembled surfactant aggregates. *Langmuir* **35**, 14151–14172 (2019).
30. S. Chakraborty, T. I. Morozova, J. L. Barrat, Intrinsically disordered proteins can behave as different polymers across their conformational ensemble. *J. Phys. Chem. B* **129**, 2359–2369 (2025).
31. M. Zhou *et al*., A theoretical and experimental investigation of the effect of sodium dodecyl sulfate on the structural and conformational properties of bovine β-casein. *Soft Matter* **15**, 1551–1561 (2019).
32. H. Farrell, E. Wickham, J. Unruh, P. Qi, P. Hoagland, Secondary structural studies of bovine caseins: Temperature dependence of β-casein structure as analyzed by circular dichroism and FTIR spectroscopy and correlation with micellization. *Food Hydrocoll.* **15**, 341–354 (2001).
33. B. R. Dumas, G. Brignon, F. Grosclaude, J. C. Mercier, Primary structure of bovine β casein: Complete sequence. *Eur. J. Biochem.* **25**, 505–514 (1972).
34. S. Dauphas *et al*., The supramolecular organisation of β-casein: Effect on interfacial properties. *Food Hydrocoll.* **19**, 387–393 (2005).
35. C. Moitzi, I. Portnaya, O. Glatter, O. Ramon, D. Danino, Effect of temperature on self-assembly of bovine β-casein above and below isoelectric ph. Structural analysis by cryogenic-transmission electron microscopy and small-angle x-ray scattering. *Langmuir* **24**, 3020–3029 (2008).
36. J. O'Connell, V. Grinberg, C. de Kruif, Association behavior of β-casein. *J. Colloid Interface Sci.* **258**, 33–39 (2003).
37. C. Cragnell *et al*., Bovine β-casein has a polydisperse distribution of equilibrium micelles. *Food Hydrocoll.* **70**, 65–68 (2017).
38. H. Srinivasan, V. K. Sharma, S. Mitra, Breaking the Brownian barrier: Models and manifestations of molecular diffusion in complex fluids. *Phys. Chem. Chem. Phys.* **26**, 29227–29250 (2024).
39. H. Srinivasan, V. Sharma, S. Mitra, R. Mukhopadhyay, Heterogeneity in dynamics of dioctadecyldimethylammonium bromide bilayers: Molecular dynamics simulation and neutron scattering study. *J. Phys. Chem. C* **122**, 20419–20430 (2018).
40. D. Vural, L. Hong, J. C. Smith, H. R. Glyde, Motional displacements in proteins: The origin of wave-vector-dependent values. *Phys. Rev. E* **91**, 052705 (2015).
41. D. Di Bari *et al*., Diffusive dynamics of bacterial proteome as a proxy of cell death. *ACS Cent. Sci.* **9**, 93–102 (2023).
42. B. Caviglia *et al*., Cytoplasmic fluidity and the cold life: Proteome stability is decoupled from viability in psychrophiles. *Nat. Commun.* **16**, 10345 (2025).
43. R. Metzler, J. H. Jeon, A. G. Cherstvy, E. Barkai, Anomalous diffusion models and their properties: Non-stationarity, non-ergodicity, and ageing at the centenary of single particle tracking. *Phys. Chem. Chem. Phys.* **16**, 24128–24164 (2014).
44. F. Höfling, T. Franosch, Anomalous transport in the crowded world of biological cells. *Rep. Prog. Phys.* **76**, 046602 (2013).
45. C. Holt, *Structure and Stability of Bovine Casein Micelles* (Elsevier, 1992), p. 63–151.
46. A. Post, B. Arnold, J. Weiss, J. Hinrichs, Effect of temperature and ph on the solubility of caseins: Environmental influences on the dissociation of αs-and β-casein. *J. Dairy Sci.* **95**, 1603–1616 (2012).
47. A. Aschi, P. Calmettes, M. Daoud, R. Douillard, A. Gharbi, Micelle formation in β-casein solutions. *Polymer* **50**, 6024–6031 (2009).
48. I. Portnaya *et al*., Micellization of bovine β-casein studied by isothermal titration microcalorimetry and cryogenic transmission electron microscopy. *J. Agric. Food Chem.* **54**, 5555–5561 (2006).
49. C. J. Oldfield, A. K. Dunker, Intrinsically disordered proteins and intrinsically disordered protein regions. *Annu. Rev. Biochem.* **83**, 553–584 (2014).
50. J. Zhang *et al*., The effects of pH, temperature, and buffer concentration on the self-assembling behavior, secondary structure, and surface hydrophobicity of donkey and bovine β-casein. *Food Chem.* **433**, 137285 (2024).
51. S. Ossowski *et al*., Aggregation behavior of bovine κ-and β-casein studied with small angle neutron scattering, light scattering, and cryogenic transmission electron microscopy. *Langmuir* **28**, 13577–13589 (2012).
52. C. G. de Kruif, T. Huppertz, V. S. Urban, A. V. Petukhov, Casein micelles and their internal structure. *Adv. Colloid Interface Sci.* **171–172**, 36–52 (2012).
53. T. Seydel *et al*., Data from "Casein as a model intrinsically disordered protein: Impact of salt on the internal diffusive dynamics in solution". ILL. https://doi.ill.fr/10.5291/ILL-DATA.9-13-1046. Deposited 19 April 2023.
54. T. I. Morozova, N. A. García, J. L. Barrat, Temperature dependence of thermodynamic, dynamical, and dielectric properties of water models. *J. Chem. Phys.* **156**, 126101 (2022).
55. T. I. Morozova, N. A. García, J. L. Barrat, Sequence length controls coil-to-globule transition in elastin-like polypeptides. *J. Phys. Chem. Lett.* **15**, 10757–10762 (2024).
56. G. Goret, B. Aoun, E. Pellegrini, Mdanse: An interactive analysis environment for molecular dynamics simulations. *J. Chem. Inf. Model.* **57**, 1–5 (2017).
57. M. Grimaldo, F. Roosen-Runge, F. Zhang, T. Seydel, F. Schreiber, Diffusion and dynamics of γ-globulin in crowded aqueous solutions. *J. Phys. Chem. B* **118**, 7203 (2014).
58. F. Roosen-Runge *et al*., Protein self-diffusion in crowded solutions. *Proc. Natl. Acad. Sci. U.S.A.* **108**, 11815–11820 (2011).
59. I. Mosca *et al*., Biophysical determinants for the viscosity of concentrated monoclonal antibody solutions. *Mol. Pharm.* **20**, 4698–4713 (2023).
60. J. Pérez, J. M. Zanotti, D. Durand, Evolution of the internal dynamics of two globular proteins from dry powder to solution. *Biophys. J.* **77**, 454–469 (1999).
61. K. Singwi, A. Sjölander, Diffusive motions in water and cold neutron scattering. *Phys. Rev.* **119**, 863 (1960).
62. J. Qvist, H. Schober, B. Halle, Structural dynamics of supercooled water from quasielastic neutron scattering and molecular simulations. *J. Chem. Phys.* **134**, 144508 (2011).
63. J. L. Barrat, J. P. Hansen, *Basic Concepts for Simple and Complex Liquids* (Cambridge University Press, 2003).
64. T. I. Morozova, N. A. García, O. Matsarskaia, F. Roosen-Runge, J. L. Barrat, Structural and dynamical properties of elastin-like peptides near their lower critical solution temperature. *Biomacromolecules* **24**, 1912–1923 (2023).
65. G. K. Batchelor, Brownian diffusion of particles with hydrodynamic interaction. *J. Fluid Mech.* **74**, 1–29 (1976).
66. B. Cichocki, B. U. Felderhof, Long-time self-diffusion coefficient and zero-frequency viscosity of dilute suspensions of spherical Brownian particles. *J. Chem. Phys.* **89**, 3705–3709 (1988).
67. A. J. Banchio, G. Nägele, Short-time transport properties in dense suspensions: From neutral to charge-stabilized colloidal spheres. *J. Chem. Phys.* **128**, 104903 (2008).
68. A. Thurn, W. Burchard, R. Niki, Structure of casein micelles I. Small angle neutron scattering and light scattering from β-and χ-casein. *Colloid Polym. Sci.* **265**, 653–666 (1987).
69. K. Kajiwara *et al*., Micellar structure of β-casein observed by small-angle x-ray scattering. *Biochim. Biophys. Acta BBA Protein Struct. Mol. Enzymol.* **955**, 128–134 (1988).
70. A. Tokuhisa, Y. Joti, H. Nakagawa, A. Kitao, M. Kataoka, Non-gaussian behavior of elastic incoherent neutron scattering profiles of proteins studied by molecular dynamics simulation. *Phys. Rev. E* **75**, 041912 (2007).
71. M. Jasnin, M. Moulin, M. Haertlein, G. Zaccai, M. Tehei, In vivo measurement of internal and global macromolecular motions in *Escherichia coli*. *Biophys. J.* **95**, 857–864 (2008).
72. L. Porcar *et al*., Formation of the dynamic clusters in concentrated lysozyme protein solutions. *J. Phys. Chem. Lett.* **1**, 126–129 (2010).
73. M. K. Braun *et al*., Crowding-controlled cluster size in concentrated aqueous protein solutions: structure, self-and collective diffusion. *J. Phys. Chem. Lett.* **8**, 2590–2596 (2017).
74. S. von Bülow, M. Siggel, M. Linke, G. Hummer, Dynamic cluster formation determines viscosity and diffusion in dense protein solutions. *Proc. Natl. Acad. Sci. U.S.A.* **116**, 9843–9852 (2019).
75. M. Grimaldo *et al*., Salt-induced universal slowing down of the short-time self-diffusion of a globular protein in aqueous solution. *J. Phys. Chem. Lett.* **6**, 2577–2582 (2015).
76. A. Girelli *et al*., Coherent x-rays reveal anomalous molecular diffusion and cage effects in crowded protein solutions. *Nat. Commun.* **16**, 10814 (2025).
77. T. A. Waigh, N. Korabel, Heterogeneous anomalous transport in cellular and molecular biology. *Rep. Prog. Phys.* **86**, 126601 (2023).
78. G. M. Whitesides, B. Grzybowski, Self-assembly at all scales. *Science* **295**, 2418–2421 (2002).
79. M. Appel, B. Frick, A. Magerl, A flexible high speed pulse chopper system for an inverted neutron time-of-flight option on backscattering spectrometers. *Sci. Rep.* **8**, 13580 (2018).
80. B. Frick, E. Mamontov, L. V. Eijck, T. Seydel, Recent backscattering instrument developments at the ILL and SNS. *Z. Phys. Chem.* **224**, 33–60 (2010).
81. D. Van Der Spoel *et al*., Gromacs: Fast, flexible, and free. *J. Comput. Chem.* **26**, 1701–1718 (2005).